Tunable, multi-modal, and multi-directional vibration energy harvester based on three-dimensional architected metastructures

Rujie Sun[1#], Qinyu Li[1#], Jianfei Yao[2,3], Fabrizio Scarpa[1,a], Jonathan Rossiter[4,5,a]

[1]*Bristol Composites Institute (ACCIS), University of Bristol, Bristol, BS8 1TR, UK*

[2]*Beijing Key Laboratory of Health Monitoring and Self-recoverying for High-end Mechanical Equipment, Beijing University of Chemical Technology, Beijing 100029, China*

[3]*College of Mechanical and Electrical Engineering, Beijing University of Chemical Technology, Beijing 100029, China*

[4]*Department of Engineering Mathematics, University of Bristol, Bristol, BS8 1UB, UK*

[5]*Bristol Robotics Laboratory, University of Bristol, Bristol, BS16 1QY, UK*

[a]Authors to whom correspondence should be addressed: F.Scarpa@bristol.ac.uk and Jonathan.Rossiter@bristol.ac.uk

[#]These authors contributed equally to this work

Abstract

Conventional vibration energy harvesters based on two-dimensional planar layouts have limited harvesting capacities due to narrow frequency bandwidth and because their vibratory motion is mainly restricted to one plane. Three-dimensional architected structures and advanced materials with multifunctional properties are being developed in a broad range of technological fields. Structural topologies exploiting compressive buckling deformation mechanisms however provide a versatile route to transform planar structures into sophisticated three-dimensional architectures and functional devices. Designed geometries and Kirigami cut patterns defined on planar precursors contribute to the controlled formation of diverse three-dimensional forms. In this work, we propose an energy harvesting system with tunable dynamic properties, where piezoelectric materials are integrated and strategically designed into three-dimensional compliant architected metastructures. This concept enables energy scavenging from vibrations not only in multiple directions but also across a broad frequency bandwidth, thus increasing the energy harvesting efficiency. The proposed system comprises a buckled ribbon with optional Kirigami cuts. This platform enables the induction of vibration modes across a wide range of resonance frequencies and in arbitrary directions, mechanically coupling with four cantilever piezoelectric beams to capture vibrations. The multi-modal and multi-directional harvesting performance of the proposed configurations has been demonstrated in comparison with planar systems. The results suggest this is a facile strategy for the realization of compliant and high-performance energy harvesting and advanced electronics systems based on mechanically assembled platforms.

Keywords: Energy harvesting; Kirigami; Multi-modal; Multi-directional; Vibration

1. Introduction

Sustainable energy systems have been investigated to mitigate the impact on the environment. Energy harvesting techniques have received significant attention in recent years to efficiently convert various renewable and sustainable energy sources into electricity, and their potential applications have been demonstrated in various emerging areas, including implantable biomedical devices[1], wireless sensor networks for the Internet of Things [2] and wearable electronics [3]. Various energy forms from the environment have been considered for harvesting, such as electrochemical [4], thermal [5], radio frequency [6], solar [7], and vibration sources [8]. Vibration in particular constitutes a ubiquitous source of energy, being found during human daily activity, wind flow, ambient noise, vehicle transportation and many other man-made activities. Vibration energy harvesting has been evaluated and exploited over decades to achieve vibration-to-electricity conversion. Mechanisms employing electromagnetic [9], electrostatic [10], and piezoelectric transduction [11] are widely used. The methods and principles for mechanical kinetic energy harvesting are summarized in [12]. The piezoelectric transduction effect, converting random vibration into electric voltage, is particularly adopted due to its scalability, simple architecture, high power density and energy conversion efficiency [13]. These characteristics make piezoelectric energy harvesting appealing for a broad range of applications in the areas of self-powered systems and active sensors [14].

A simple and extensively studied energy harvester is the cantilever-type piezoelectric vibration beam [15]. This type of energy harvesting system largely relies on exploiting the dynamic

deformation of the beam at resonance. The first bending mode of the beam is normally used for energy harvesting purposes, while higher-order modes are usually ignored due to their high frequency and low response amplitude. Environmental vibrations, however, are intrinsically random in directions and broadband. The mismatch of the resonant frequency between the harvester and the ambient excitation drastically reduces the power output. The above single-degree-of-freedom (SDOF) harvester cannot cover the frequency range of environmental vibrations because of its narrow bandwidth. To overcome this limitation, various approaches have been explored to increase the power output [16]. Multiple-degree-of-freedom (MDOF) systems have also been investigated to broaden the bandwidth by coupling with multiple resonant modes. State-of-art technologies in energy harvesting can be categorized into three types: magnetic coupling, mechanical coupling, and combinations of the two. Magnetic coupling is based on two or more repulsively or attractively coupled neighbouring components. It can be used in different configurations, such as E-shape with three uniform beams [17], arrayed cantilevered beams with variable sizes [18], and flextensional systems [19]. Mechanical coupling, however, uses mechanical components, i.e. tip mass [20], tip beam [21], double-branched beam [22], proof mass [23], butterfly-inspired structure [24], and binder clip structure [25], as couple different parts in the system. The third method is to combine the advantages of these two coupling systems to develop multi-modal systems. For example, a seesaw-type energy harvester for ambient vibration was exploited in [26]. This system consists of a primary beam with a U-shape groove mechanically coupled with an internal cantilever beam. A permanent magnet is fixed at the primary beam to generate the potential magnetic coupling energy. Other configurations, such as multimodal hybrid energy harvester with four coupled symmetrical beams [27] and U-shape micro-cantilever [28], were also investigated. Although these MDOF harvesters can increase the operational bandwidth, they usually scavenge energy along a single direction only, therefore reducing energy harvesting efficiency in multi-directional environmental vibrations. There is therefore a need for more effective multi-directional and broader-bandwidth energy harvesting structures.

One route to better harvesters is through the extension or projection of two-dimensional (2D) structures into the third dimension. Three-dimensional (3D) structures can be mechanically assembly by compressive buckling [29]. In this mechanically assembly method, precisely patterns can be defined on a variety of materials in their 2D forms, and then transformed into targeted 3D configurations through controlled compressive buckling. This design and manufacturing method has expanded the material options and length scales in 3D structural designs. Previous research has worked on several potential applications with various 3D systems based on this mechanically-assembled method, including soft electronics [30], microrheological devices [31], precise characterization of thin polymer films [32], and tunable dynamic systems [33]. However, research to design a novel type of vibration platform with more efficient multi-directional energy harvesting is limited.

In this paper, we propose a 3D structurally tunable platform for multi-modal and multi-directional energy harvesting for low-frequency vibration based on 2D-to-3D assembly by compressive buckling. The 3D platform described here allows for a mechanical coupling between multiple parts of the structure, thereby delivering a multimodal and multi-degree-of-freedom (MDOF) system. The assembled 3D metastructure provides routes to improve the operational bandwidth and energy harvesting performance in the presence of multi-directional vibrations. A zigzag Kirigami cut pattern is applied to the buckled ribbon that is induced during compressive assembly to enhance the dynamic performance. Modal analysis using finite element methods is carried out to study the proposed 3D metastructures, and the structural response is verified by comparing the numerical results with data from a series of vibration

tests. The tunable properties are also evaluated for different pre-strains to the compressive buckling and by changing the topology of the Kirigami cut pattern. A comparative study between the proposed 3D metastructures and conventional planar systems is carried out. 3D piezoelectric energy harvesters based on the proposed metastructure design are fabricated and tested under multi-directional vibration loading. Finally, the performances of the proposed energy harvesting devices are evaluated for wind energy harvesting under a range of wind directions and air speeds.

2. Design and experimental setup

2.1 Device configuration design and description

The 3D metastructures developed here are based on the mechanically assembly of 2D planar structures subjected to compressive buckling. The configuration can be designed and patterned in its 2D precursor form using techniques including photolithography and laser cutting. The 2D pattern is then locally translated in the 2D plane, causing it to buckle at pre-determined points into a 3D structure. As depicted in Fig. 1, the proposed 3D energy harvester platform is developed from patterning planar polyethylene terephthalate (PET) films by laser cutting, which is then assembled into pre-defined 3D configurations through controlled compressive buckling.

In our proposed configurations, four cantilever beams are mechanically coupled with each other through a central bridge which has been compressively buckled. This design enables the coupled beams to provide a compact MDOF energy harvesting system, and it also improves the broadband performance of conventional MDOF systems made from independent cantilever beams. In addition, the proposed system can also capture vibration energy from multiple directions in three dimensions due to the presence of the buckled 3D structures. Compared with planar systems, the proposed 3D structures can be designed to be particularly sensitive to multi-directional ambient vibrations. Four representative vibration modes of the 3D buckled structure with patterned Kirigami cuts on the buckled beams are presented in Fig. 2. The three modes in Fig. 2(a)-(c) can be excited by vibrations from three orthogonal directions, while the mode in Fig. 2(d) can be excited by torsion motions about the z axis. These characteristics demonstrate that the proposed 3D tunable system has the potential to be applied for multi-directional and multi-modal vibrational energy harvesting.

The Kirigami cuts on the buckled beams is optional, and that provides one more possibility to tune the structural performances and meeting different applications. As illustrated in the following part, the introduction of these Kirigami cuts induce more flexibility of the structure, thus reducing the resonance frequencies.

2.2 Experimental setup

A vibration platform is set up to investigate the dynamic characteristics of the 3D MDOF systems and the voltage outputs of the fabricated energy harvesters, as shown in Fig. 3. The 3D metastructures are bonded onto an acrylic base plate, which is then mounted on top of a shaker (LDS shaker system) that provides the base excitation. An accelerometer (PCB Piezotronics 333M07) is placed on the acrylic plate for the measurement of the base accelerations. The vibration shaker is controlled by the signal produced by a multifunction I/O device (NI USB-6211) and amplified by a power amplifier (LDS PA25E).

For the dynamic analysis of the 3D metastructures, a single-point vibrometer (Polytec PDV-100) is used to capture the structural velocities during the dynamic tests. The accelerometer output is first processed through a signal coupler (Kistler 5134), and then recorded by a NI data acquisition card USB-6211. The signal from the laser vibrometer is directly connected to an input channel of the same card. A custom Matlab (R2017b) script is used for control and signal processing.

For the electrical performance evaluation, the generated voltage output of the 3D energy harvester is recorded by a multi-channel oscilloscope (PicoScope 2405A). A sinusoidal waveform with controlled amplitude is generated by the NI USB-6211 card to excite the vibration shaker with sweep frequencies at different vibration levels. The voltage outputs of the energy harvester under a frequency sweep test are investigated.

For the evaluation of wind energy harvesting, an electric fan is used to generate different levels of wind speeds, recorded by an anemometer (Sealey TA070). The voltage outputs of the energy harvester at different levels of air flow and different directions are recorded by the oscilloscope.

2.3 Device fabrication

We adopt here a direct and facile method to fabricate the 3D metastructure and its associated energy harvester. The substrate is a PET film with a thickness of 125 μm, and the 2D configuration is designed using Auto CAD (Autodesk 2018). The PET film is cut into the designed layout by a laser engraver (Speedy 100). An acrylic plate is then cut with mounting pads for the PET film arranged such that the designated 3D structure can be generated when the film is bonded to the frame at those points. The pre-strain is controlled by the distance between these two mounting pads. For example, herein the length of the 2D precursors is 60 mm, and 30% pre-strain can be achieved when the distance between the two mounting pads is reduced to 42 mm. Additional Kirigami patterns can be made on the two middle of the PET beams by the laser engraver. The beams are then buckled to assemble into a 3D configuration. A piece of laser reflective film (5mm × 3mm, Testo Reflective Tape) is bonded on the tip of each of the four cantilever beams to enhance the scatter of the laser from the vibrometer.

In order to turn the PET structures into an energy harvester, an electrically conductive adhesive (3M 9707) is firstly bonded onto the middle area of the PET substrate as a common bottom electrode. Four polyvinylidene fluoride (PVDF) films (28 μm of thickness, 16 mm × 4 mm, electrodes: 70 nm / 10 nm of copper / nickel, TE Connectivity, its piezoelectric property is: relative permittivity: 12; d_{31} constant: 23 pC/N; d_{33} constant: -33 pC/N) are cut using a die-cutting machine (Cricut Explore Air 2) then bonded onto the top surface of each of the four cantilever arms using acrylic adhesive (3M 7952MP). Copper wires are bonded on the top electrode surface of the PVDF film using silver conductive paint (Electrolube, SCP03B). A second wire is connected to the common bottom electrode.

The cutting of Kirigami patterns and the integration of PVDF films are performed on the 2D precursors. The planar structure is assembled into a defined 3D configuration by compressive buckling under different pre-strains and by bonding the structures onto the specified areas of the acrylic plate. Fig. 4 shows the precursor 3D structure, laminar components and fully assembled 3D structure.

One of the advantages of the proposed system is its low-cost fabrication process and materials. We have introduced Kirigami cuts by laser to pattern the 2D PET film, and then mechanically

assembled 2D structures into 3D configurations. The whole process does not require complex or expensive equipment, and could be extended to different types of substrates, making it cost efficient. The inherent costs of the base materials are low.

3. Results and Discussions

3.1 Vibration mode analysis

In this work, we propose two types of metastructure platforms for the energy harvester: a 3D buckled structure and a modified 3D configuration with additional Kirigami cut patterns. Numerical simulations based on finite element analysis are performed to study the dynamic characteristics of the structures. A 2D shell element (S4R) model in Abaqus (Abaqus/Standard 6.14) is used for the models with PET material properties (density 1.38 g/cm^3, modulus 6980 MPa, Poisson ratio 0.44, and thickness 125 μm). Two main steps are defined in the simulation study: a static analysis to transform the planar structure into its 3D configuration, followed by a frequency analysis of the buckled 3D structure.

As shown in Fig. 5, the 3D buckled structure without Kirigami cuts possesses the first four modes at low frequency range (1 - 50 Hz). The four cantilever beams are coupled with each other, and that generates diverse vibration modes within this low frequency range. The behaviors of these coupled beams in different positions are either in phase or counter phase with each other. In the first and second modes, the beams in positions 1 and 2 deform in counter phase, while they are in phase for the third and fourth modes. However, the beams in positions 1 and 3 deform in phase in the first and fourth modes, and in counter phase in the second and third modes.

A similar study is performed on the modified 3D metastructures (Fig. 6). We define a linear Kirigami cut pattern on the buckled beams to further tune the dynamic performances of these 3D structures. In this case six vibration modes occur within the same frequency range (1 Hz to 50 Hz). The introduction of the Kirigami cuts triggers a higher number of normal modes and reduces the resonant frequencies of the system, compared with the structure without Kirigami cuts. The modified structure also features clear vibration modes in different directions: translational modes (the 1st mode along the x direction, the 2nd and 6th modes along the y direction, and the 5th mode along z direction) and torsion modes (the 3rd and 4th modes along z direction). These results show that the proposed 3D metastructure could provide a promising platform to harvest vibrational energy with broad frequency bandwidth and along multiple directions. It is also evident from the modal analysis that the voltage generated from each piezoelectric film (the placements of which are shown in Fig. 4(c)) should be scavenged individually to avoid charge cancellation effect due to the phase difference in the resonant modes.

We then performed linear buckling analysis to evaluate the dynamic features of the structure. A concentrated unit force along x, y, and z directions was applied on two representative position, one on the beam tip and the other on the central point of the structure (Fig. S1 in supplementary information). The buckling reserve factors are summarized in Table 1. They are however lower than 1 due to the scale of the structure (around 2 g in weight), and that suggests that for loading-bearing capabilities it should include a sizeable safety factor in future designs. Besides, the introduction of Kirigami cuts on the buckled beams would increase the structural flexibility, but however diminish the structure steadiness.

3.2 Measurement of structural characteristics

A series of vibration tests have been carried out to verify the simulation results and validate the feasibility of the proposed designs by comparing the structural performances of the proposed 3D metastructure with those of conventional planar systems.

We firstly evaluated the performance of the 3D buckled structure without Kirigami cuts. Modal analysis has been carried out by evaluating the vibration transmissibility (TR) of the structures. The vibration transmissibility is defined as the ratio of output (the beam tip acceleration) to input (the shaker acceleration). The shaker acceleration is sensed by the accelerometer placed on the shaker base. The velocity of the beam tips is first measured by the laser vibrometer, and further converted into acceleration by differentiation. The shaker is excited by a frequency sweep from 1 to 50 Hz and an increment of 0.3 Hz /s. The tip velocity is then numerically converted into acceleration before the transmissibility calculations. As shown in Fig. 7, the Bode plot of the transmissibility along the z direction confirms the results from the simulations: four resonant modes are present between 1 and 50 Hz, with the predicted natural frequencies comparing well with the experimental results (Table 2). The phase extracted from the experimental TR (Fig. S2 in supplementary information) also validates the prediction from the simulations, i.e. the coupled beams deform either in phase or counter phase in the different resonant modes. To demonstrate the superior performance of our platform under multi-directional vibrations, a series of vibration tests were carried out. The position of the shaker remained the same while the acrylic base was adjusted to apply three orthogonal directional vibrations to the structures, as shown in Fig. 8. The same input as the previous TR test (sweep frequency and amplitude) were applied on the shaker. Fig. 9 shows the results of the structural transmissibility under the three directional vibrational excitations. The 3D buckled metastructure can generate significant output in both x and y directions, while the output along z direction dominates. The structure also induces higher amplitudes and a lower resonant frequency in the x direction compared to that along the y direction.

A similar study was performed on the modified 3D metastructure with additional Kirigami cuts. As demonstrated by the numerical simulations, the structural transmissibility of the modified structure exhibits a more diverse modal behavior compared to the 3D structure without Kirigami cuts. Six vibration modes are clearly present in the experimental Bode plot (Fig. 10). The phase differences in the four beams in different modes also exhibit similar relationships, either in phase or counter phase (see supplementary information Fig. S3). The modified 3D metastructure also shows advantages in terms of transmissibility, and the structure can generate comparable transmissibility magnitudes along the three directions, as shown in Fig. 11. Vibrations along the x direction have the highest amplitudes at low frequencies. Higher amplitudes at high frequencies are observed in vibrations along the z direction, while two transmissibility peaks are observed in the y directional at the low (approx. 23 Hz) and high (approx. 42 Hz) ends of the frequency spectrum. A comparison between the 3D structure with and without the Kirigami cuts is also reported in supplementary information (Fig. S4). It can be clearly seen that the introduction of the Kirigami cuts not only tends to increase the magnitude of the resonance frequencies, but it also generates more vibration modes within the same frequency range. Moreover, The Kirigami cut patterns also make the structure more compliant along the x and y directions.

To demonstrate the superior characteristics of the proposed 3D metastructure, a comparative study has been performed with the conventional planar structures. Two corresponding flat structures were investigated, a planar structure with four mechanically coupled beams (Fig.

12a) and a modified planar structure with Kirigami cuts (Fig. 12b). Modal analysis was carried out on these two structures respectively, and the structural transmissibility in multi-directions was determined. Both structural configurations show that the transmissibility in x and y directions is negligible compared with the z direction, which confirms that such a type of planar design is only suitable to the energy harvesting in one vibration direction. Similarly, the Kirigami cuts also reduce the resonance frequency of the structure.

In addition to the advantages of multi-modal and multi-directional vibration energy harvesting capabilities, the proposed structure can be tuned by assembly parameters, such as the pre-strain, to control the buckling. We investigated the dynamic properties of the structures buckled with different pre-strains, 10 %, 20 %, and 30 %, as seen in Fig. 13(a). Their structural transmissibility is calculated and compared in Fig. 13(b)-(d). The increase of the pre-strain leads to an increase in resonant frequencies when the structure is subjected to the x directional vibration. The opposite however occurs when the dynamic loading is exerted along the y direction: as the pre-strain increases, the resonant frequencies decrease. The transmissibility of the metastructure does not however exhibit a clear dependence versus the level of pre-strain when subjected to the z directional vibration.

3.3 Energy harvesting from multi-directional vibration

Following the validation of the baseline configuration of the 3D metastructures, we designed and fabricated two types of energy harvesters using the presented 3D platform. A series of vibration tests have been carried out to analyze the voltage outputs from the devices. The structures discussed herein have been buckled with a pre-strain level of 30 %. The voltage outputs along three orthogonal directions under different vibrational amplitudes for the 3D structure without Kirigami cuts are shown on the left of Fig. 14. Compared to the pure PET structure discussed in Section 3.2, these energy harvesting devices are stiffer overall (i.e. they have higher resonant frequencies) due to the integration of the relatively stiff PVDF films with the substrate. A frequency sweep from 1 Hz to 120 Hz was applied. With the increase of the amplitude of the shaker input, the voltage amplitudes increase accordingly. Along the x direction, the voltage outputs have a peak around 100 Hz, while for the y direction, the voltage output exhibits a wider bandwidth between 40 Hz and 80 Hz, and for the z direction vibration two peaks are seen within the ranges of 40 Hz – 60 Hz and 80 Hz – 100 Hz respectively. A comparative study was performed to validate the voltage output from the piezoelectric films in supplementary information (Fig S6). The voltage output is normalised by the acceleration with the unit of V/g. The laser vibrometer is used to capture the structural deformation of the device and to calculate the structural transmissibility, using a similar procedure to Section 3.2. The transmissibility along the three directions is compared with the corresponding voltage output, and modal analysis confirms that the resonant frequencies from structural analysis and voltage output are consistent.

The voltage outputs for the modified device with Kirigami cuts are analyzed under a series of vibration tests, and shown on the right of Fig. 14. We compared the voltage output for multi-directional vibrations and different shaker vibration amplitudes. The device can generate comparable voltage outputs in all three orthogonal directions, and the voltage amplitude increases with vibration amplitude. For x and z directional vibrations, the device has a broad bandwidth between 40 Hz and 60 Hz, and for the z directional vibration, an additional output peak is observed in the range 80 Hz to 100 Hz. A comparative study between the structural analysis and voltage output is conducted with the results summarized in supplementary

information (Fig. S7), and it is shown that the resonant frequencies based on these two measurements match well.
The acceleration input from the shaker is given in Fig. 15(b) as a high amplitude. It gradually increases to the given value of 0.36g. Under this condition, the voltage output of the metastructure can reach 2V, as shown in Fig.15(a).

We further investigated the voltage generation performance of the conventional energy harvester based on planar configurations. Two types of planar energy harvesters were analyzed: a planar structure with four coupled piezoelectric beams; and a modified planar structure with additional Kirigami cuts on the central beams. A frequency sweep was conducted under multi-directional vibration. As seen in the Supplementary Information Fig. S8, both planar devices show good performance in harvesting energy along the z axis, while along the x and y directions the devices fail to transduce significant vibration. Structural analysis in the z direction confirms the frequency responses embodied in the voltage outputs (see supplementary information Fig. S9). In contrast, the proposed 3D harvesting devices have been demonstrated to be promising in multi-modal and multi-directional vibration energy harvesting.

3.4 Demonstration of wind energy harvesting

The structural analysis and voltage outputs have validated the supervisor performance of the presented designs. In this section, the voltage generation capacities of the devices in a custom wind environment are evaluated. We use a commercial electric fan as the wind source, which can provide different wind speeds. In real applications, the wind direction is typically time-varying, thus requiring the energy harvesting device to possess the ability to extract energy from air flow from different directions. Herein, two different wind directions were applied, in-plane (x-y plane) and out-of-plane (perpendicular to x-y plane). For the in-plane air flow, three representative angles were used, as seen in Fig. 16(a), where α defines the in-plane wind angle with respect to the x axis. The wind test for the 3D energy harvester with Kirigami cuts under two levels of wind speeds are summarized as frequency domain responses in Fig. 16(b)-(c), with low speed of 1.9 m/s and high speed of 2.2 m/s. It can be seen that the device has a broad low frequency bandwidth of around 60 Hz for both in-plane and out-of-plane winds. The voltage outputs from the out-of-plane wind features the largest amplitude as the wind directly acts upon the four beams lying orthogonal to that direction. For the in-plane wind, the $\alpha = 0°$ angle wind is more efficient than the $\alpha = 90°$ angle wind in inducing vibrations, and the generated voltage under the 45° wind has a similar frequency response but with a lower amplitude. For the 3D energy harvesting system without Kirigami cuts, the results in the above wind environment are summarized in supplementary information (Fig. S9).

The PVDF film used in this paper has a small effective area which is 12 mm × 4 mm. In terms of the practical applications, the power capacity could be readily improved. The presented method is based on Kirigami designs to achieve 3D multi-modal structures. By scaling up the dimensions with lase cutting, the voltage output could be further enhanced.

4. Conclusion

A novel system based on 3D architected metastructures is presented for low-frequency vibration energy harvesting. Two types of 3D configurations either with or without additional Kirigami cuts have been designed and investigated, and a combined numerical and experimental study has demonstrated that this design has supervisor performances in multi-directional vibrations and features a broad frequency bandwidth within a low frequency range.

Moreover, the dynamic properties of the proposed 3D structure are highly tunable by changing the pre-strain of the structural buckling or through the introduction of Kirigami cut patterns. Based on the 3D structural platform, we designed and fabricated a series of energy harvesters, and dynamic tests validate that the proposed devices exhibit significant energy harvesting capacities for multi-direction low-frequency vibrations. The fabrication process of these structures is simple and allows for various geometric designs on the 2D precursor, with mechanical assembly into the defined 3D architectures. These features have been validated in a custom wind environment with effective energy harvesting from different directional winds and show frequency responses with broad bandwidths. The 3D vibration systems presented in this work provide promising insights in high-performance energy harvesters. In real applications, tunable systems are essential to meet different dynamic conditions. This can be readily achieved in the presented platform, including tunable frequency range and vibration directions, by optimizing the structural designs and geometric parameters.

Acknowledgements

This work was supported by the Engineering and Physical Sciences Research Council through the EPSRC Centre for Doctoral Training in Advanced Composites for Innovation and Science (Grant No. EP/L016028/1). R. Sun acknowledges the support from the China Scholarship Council. J. Rossiter is supported by EPSRC Grant Nos. EP/M020460/1, EP/M026388/1 and EP/R02961X/1, and the Royal Academy of Engineering under the Chair in Emerging Technologies scheme. Data are available at the University of Bristol data repository.

References:

[1] Shi B, Li Z, Fan Y. Implantable Energy-Harvesting Devices. Adv Mater 2018;30:1801511. https://doi.org/10.1002/adma.201801511.
[2] Shaikh FK, Zeadally S. Energy harvesting in wireless sensor networks: A comprehensive review. Renew Sustain Energy Rev 2016;55:1041–54. https://doi.org/10.1016/j.rser.2015.11.010.
[3] Wang J, Li S, Yi F, Zi Y, Lin J, Wang X, Xu Y, Wang ZL. Sustainably powering wearable electronics solely by biomechanical energy. Nat Commun 2016;7:12744. https://doi.org/10.1038/ncomms12744.
[4] Kim S, Choi SJ, Zhao K, Yang H, Gobbi G, Zhang S, Li J. Electrochemically driven mechanical energy harvesting. Nat Commun 2016;7:10146. https://doi.org/10.1038/ncomms10146.
[5] Nan K, Kang SD, Li K, Yu KJ, Zhu F, Wang J, Dunn AC, Zhou C, Xie Z, Agne MT, Wang H, Luan H, Zhang Y, Huang Y, Snyder GJ, Rogers JA. Compliant and stretchable thermoelectric coils for energy harvesting in miniature flexible devices. Sci Adv 2018;4:eaau5849. https://doi.org/10.1126/sciadv.aau5849.
[6] Le T, Mayaram K, Fiez T. Efficient Far-Field Radio Frequency Energy Harvesting for Passively Powered Sensor Networks. IEEE J Solid-State Circuits 2008;43:1287–302. https://doi.org/10.1109/JSSC.2008.920318.

[7] Scholes GD, Fleming GR, Olaya-Castro A, van Grondelle R. Lessons from nature about solar light harvesting. Nat Chem 2011;3:763–74. https://doi.org/10.1038/nchem.1145.
[8] Wei C, Jing X. A comprehensive review on vibration energy harvesting: Modelling and realization. Renew Sustain Energy Rev 2017;74:1–18. https://doi.org/10.1016/j.rser.2017.01.073.
[9] Beeby SP, Torah RN, Tudor MJ, Glynne-Jones P, O'Donnell T, Saha CR, Roy S. A micro electromagnetic generator for vibration energy harvesting. J Micromechanics Microengineering 2007;17:1257–65. https://doi.org/10.1088/0960-1317/17/7/007.
[10] Mitcheson PD, Miao P, Stark BH, Yeatman EM, Holmes AS, Green TC. MEMS electrostatic micropower generator for low frequency operation. Sensors Actuators A Phys 2004;115:523–9. https://doi.org/10.1016/j.sna.2004.04.026.
[11] Toprak A, Tigli O. Piezoelectric energy harvesting: State-of-the-art and challenges. Appl Phys Rev 2014;1:31104. https://doi.org/10.1063/1.4896166.
[12] Zou H-X, Zhao L-C, Gao Q-H, Zuo L, Liu F-R, Tan T, Wei K-X, Zhang W-M. Mechanical modulations for enhancing energy harvesting: Principles, methods and applications. Appl Energy 2019;255:113871. https://doi.org/10.1016/j.apenergy.2019.113871.
[13] Priya S. Advances in energy harvesting using low profile piezoelectric transducers. J Electroceramics 2007;19:167–84. https://doi.org/10.1007/s10832-007-9043-4.
[14] Yang Z, Zhou S, Zu J, Inman D. High-Performance Piezoelectric Energy Harvesters and Their Applications. Joule 2018;2:642–97. https://doi.org/10.1016/j.joule.2018.03.011.
[15] Erturk A, Inman DJ. An experimentally validated bimorph cantilever model for piezoelectric energy harvesting from base excitations. Smart Mater Struct 2009;18:25009. https://doi.org/10.1088/0964-1726/18/2/025009.
[16] Tang L, Yang Y, Soh CK. Toward Broadband Vibration-based Energy Harvesting. J Intell Mater Syst Struct 2010;21:1867–97. https://doi.org/10.1177/1045389X10390249.
[17] Lu Q, Scarpa F, Liu L, Leng J, Liu Y. An E-shape broadband piezoelectric energy harvester induced by magnets. J Intell Mater Syst Struct 2018;29:2477–91. https://doi.org/10.1177/1045389X18770871.
[18] Song H-C, Kumar P, Sriramdas R, Lee H, Sharpes N, Kang M-G, Maurya D, Sanghadasa M, Kang H-W, Ryu J, Reynolds WT, Priya S. Broadband dual phase energy harvester: Vibration and magnetic field. Appl Energy 2018;225:1132–42. https://doi.org/10.1016/j.apenergy.2018.04.054.
[19] Zou H-X, Zhang W-M, Li W-B, Wei K-X, Hu K-M, Peng Z-K, Meng G. Magnetically coupled flextensional transducer for wideband vibration energy harvesting: Design, modeling and experiments. J Sound Vib 2018;416:55–79. https://doi.org/10.1016/j.jsv.2017.11.041.
[20] Sun S, Tse PW. Modeling of a horizontal asymmetric U-shaped vibration-based piezoelectric energy harvester (U-VPEH). Mech Syst Signal Process 2019;114:467–85. https://doi.org/10.1016/j.ymssp.2018.05.029.
[21] Sun S, Tse PW. Design and performance of a multimodal vibration-based energy harvester model for machine rotational frequencies. Appl Phys Lett 2017;110:243902. https://doi.org/10.1063/1.4986477.
[22] Deng H, Du Y, Wang Z, Zhang J, Ma M, Zhong X. A multimodal and multidirectional vibrational energy harvester using a double-branched beam. Appl Phys Lett 2018;112:213901. https://doi.org/10.1063/1.5024567.
[23] Kim I-H, Jung H-J, Lee BM, Jang S-J. Broadband energy-harvesting using a two degree-of-freedom vibrating body. Appl Phys Lett 2011;98:214102. https://doi.org/10.1063/1.3595278.

[24] Lei R, Zhai H, Nie J, Zhong W, Bai Y, Liang X, Xu L, Jiang T, Chen X, Wang ZL. Butterfly-Inspired Triboelectric Nanogenerators with Spring-Assisted Linkage Structure for Water Wave Energy Harvesting. Adv Mater Technol 2019;4:1800514. https://doi.org/10.1002/admt.201800514.
[25] Wu Y, Qiu J, Zhou S, Ji H, Chen Y, Li S. A piezoelectric spring pendulum oscillator used for multi-directional and ultra-low frequency vibration energy harvesting. Appl Energy 2018;231:600–14. https://doi.org/10.1016/j.apenergy.2018.09.082.
[26] Deng H, Wang Z, Du Y, Zhang J, Ma M, Zhong X. A seesaw-type approach for enhancing nonlinear energy harvesting. Appl Phys Lett 2018;112:213902. https://doi.org/10.1063/1.5032307.
[27] Toyabur RM, Salauddin M, Cho H, Park JY. A multimodal hybrid energy harvester based on piezoelectric-electromagnetic mechanisms for low-frequency ambient vibrations. Energy Convers Manag 2018;168:454–66. https://doi.org/10.1016/j.enconman.2018.05.018.
[28] He Q, Dong C, Li K, Wang J, Xu D, Li X. A multiple energy-harvester combination for pattern-recognizable power-free wireless sensing to vibration event. Sensors Actuators A Phys 2018;279:229–39. https://doi.org/10.1016/j.sna.2018.06.022.
[29] Xu S, Yan Z, Jang K-I, Huang W, Fu H, Kim J, Wei Z, Flavin M, McCracken J, Wang R, Badea A, Liu Y, Xiao D, Zhou G, Lee J, Chung HU, Cheng H, Ren W, Banks A, Li X, Paik U, Nuzzo RG, Huang Y, Zhang Y, Rogers JA. Assembly of micro/nanomaterials into complex, three-dimensional architectures by compressive buckling. Science (80-) 2015;347:154 LP – 159. https://doi.org/10.1126/science.1260960.
[30] Jang K-I, Li K, Chung HU, Xu S, Jung HN, Yang Y, Kwak JW, Jung HH, Song J, Yang C, Wang A, Liu Z, Lee JY, Kim BH, Kim J-H, Lee J, Yu Y, Kim BJ, Jang H, Yu KJ, Kim J, Lee Jung W, Jeong JW, Song YM, Huang Y, Zhang Y, Rogers, JA. Self-assembled three dimensional network designs for soft electronics. Nat Commun 2017;8:15894. https://doi.org/10.1038/ncomms15894.
[31] Ning X, Yu X, Wang H, Sun R, Corman RE, Li H, Lee CM, Xue Y, Chempakasseril A, Yao Y, Zhang Z, Luan H, Wang Z, Xia W, Feng X, Ewoldt RH, Huang Y, Zhang Y, Rogers JA. Mechanically active materials in three-dimensional mesostructures. Sci Adv 2018;4:eaat8313. https://doi.org/10.1126/sciadv.aat8313.
[32] Nan K, Wang H, Ning X, Miller KA, Wei C, Liu Y, Li H, Xue Y, Xie Z, Luan H, Zhang Y, Huang Y, Rogers JA, Braun P V. Soft Three-Dimensional Microscale Vibratory Platforms for Characterization of Nano-Thin Polymer Films. ACS Nano 2019;13:449–57. https://doi.org/10.1021/acsnano.8b06736.
[33] Ning X, Wang H, Yu X, Soares JANT, Yan Z, Nan K, Velarde G, Xue Y, Sun R, Dong Q, Luan H, Lee CM, Chempakasseril A, Han M, Wang Y, Li L, Huang Y, Zhang Y, Rogers JA. 3D Tunable, Multiscale, and Multistable Vibrational Micro-Platforms Assembled by Compressive Buckling. Adv Funct Mater 2017;27:1605914. https://doi.org/10.1002/adfm.201605914.

Fig. 1 Schematic of the mechanical assembly of 3D structures through a compressive buckling process. Two types of platforms with and without Kirigami cuts on the buckled beams.

Fig. 2 The representative mode shapes in multi-directions. (a) and (b) in-plane translational vibration in orthotropic directions, (c) vertical translational vibration, (d) twist vibration along the vertical axis.

Fig. 3 Experimental setup for the vibration test of the proposed 3D tunable energy harvesting structure. (a) computer for system control and data recording, (b) vibration shaker, (c) accelerometer, (d) the acrylic base with the test structure mounted on it, (e) NI USB-6211 data acquisition device, (f) signal coupler, (g) shaker power amplifier, and (h) laser vibrometer.

Fig. 4 (a) the 3D vibration energy harvester with Kirigami cuts on its buckled beams. Scale bar: 10 mm. (b) the dimension of the 2D precursors. (c) the schematic illustration of the integrated energy harvesting system.

Fig. 5 The modal analysis of the 3D bucked structure without Kirigami cuts. The four cantilever beams are mechanically coupled with each other in the first four resonant modals (a)-(d) in the low frequency range below 50 Hz. The first four resonant frequencies are 24.9 Hz, 33.9 Hz, 38.2 Hz, and 39.6 Hz respectively.

Fig. 6 The modal analysis of the 3D bucked structure with Kirigami cuts on the buckled beams. The four cantilever beams are mechanically coupled with each other in the first six resonant modals (a)-(f) in the low frequency range below 50 Hz. The first six resonant frequencies are 18.9 Hz, 24.1 Hz, 30.5 Hz, 37.5 Hz, 37.6 Hz, and 43.3 Hz respectively.

Fig. 7 The phase and amplitude of the structural transmissibility for the 3D buckled structure without Kirigami cuts.

Fig. 8 The setup for multi-directional vibration test of the 3D buckled structures. (a) x-directional vibration, (b) y-directional vibration, (c) z-directional vibration.

Fig. 9 The structural characteristics of the 3D buckled structure without Kirigami cuts in multi-directional vibrations.

Fig. 10 The phase and amplitude of the structural transmissibility for the 3D buckled structure with Kirigami cuts.

Fig. 11 The structural characteristics of the 3D buckled structure with Kirigami cuts in multi-directional vibrations.

Fig. 12 The structural characteristics of the 2D planar structure in multi-directional vibrations, (a) without and (b) with Kirigami cuts.

Fig. 13 (a) The schematics of the 3D buckled structure with three pre-strains of 10 %, 20 %, and 30 %. The structure characteristics of the buckled structure with Kirigami cuts under vibrations in (b) x direction, (c) y direction, and (d) z direction.

Fig. 14 The voltage output of the buckled structure without (left) and with (right) Kirigami cuts under different vibration amplitudes in (a) x direction, (b) y direction, and (c) z direction.

Fig. 15 The voltage output of the piezoelectric films in time domain and the input acceleration of the shaker.

Fig. 16 The performance evaluation of the energy harvesting system with Kirigami cuts. (a) the schematics of in-plane and out-of-plane wind direction applied on the harvester. The comparison of the voltage output for multi-directional wind with different levels of speed. (b) low speed, and (c) high speed.

Table 1 Critical buckling factors under a concentrated unit force along x, y and z directions.

Table 2 The comparison of natural frequencies for the buckled structure without Kirigami cuts between numerical simulation and tests. The frequency range is between 1 Hz and 50 Hz.

Table 3 The comparison of natural frequencies for the buckled structure with Kirigami cuts between numerical simulation and tests. The frequency range is between 1 Hz and 50 Hz.

Fig. 1

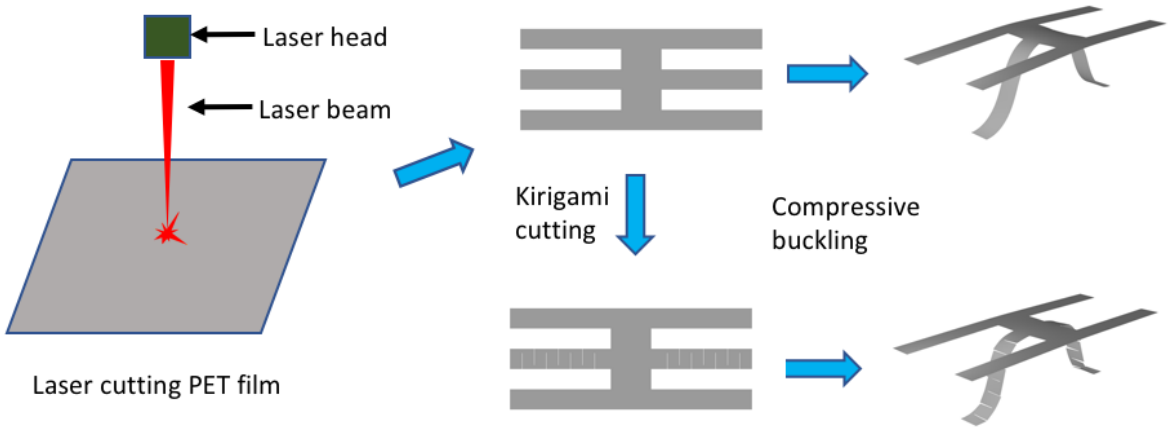
Laser head
Laser beam
Laser cutting PET film
Kirigami cutting
Compressive buckling

Fig. 2

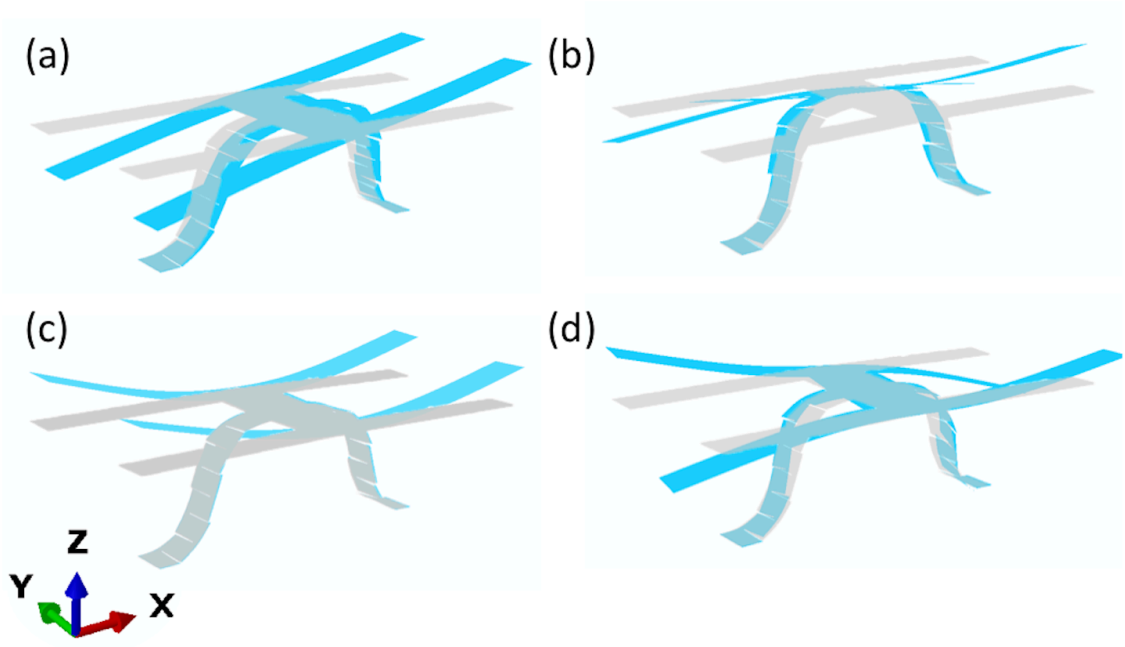
(a)
(b)
(c)
(d)
Z
Y
X

Fig. 3

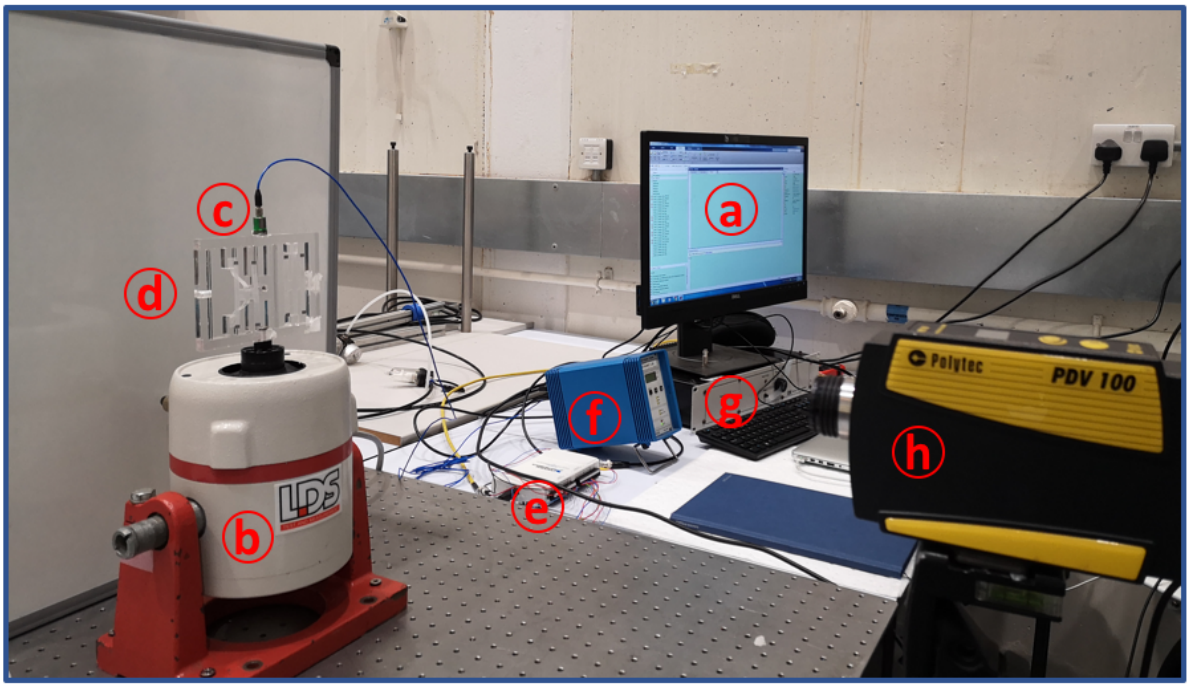
a
b
c
d
e
f
g
h
LDS
Polytec
PDV 100

Fig. 4

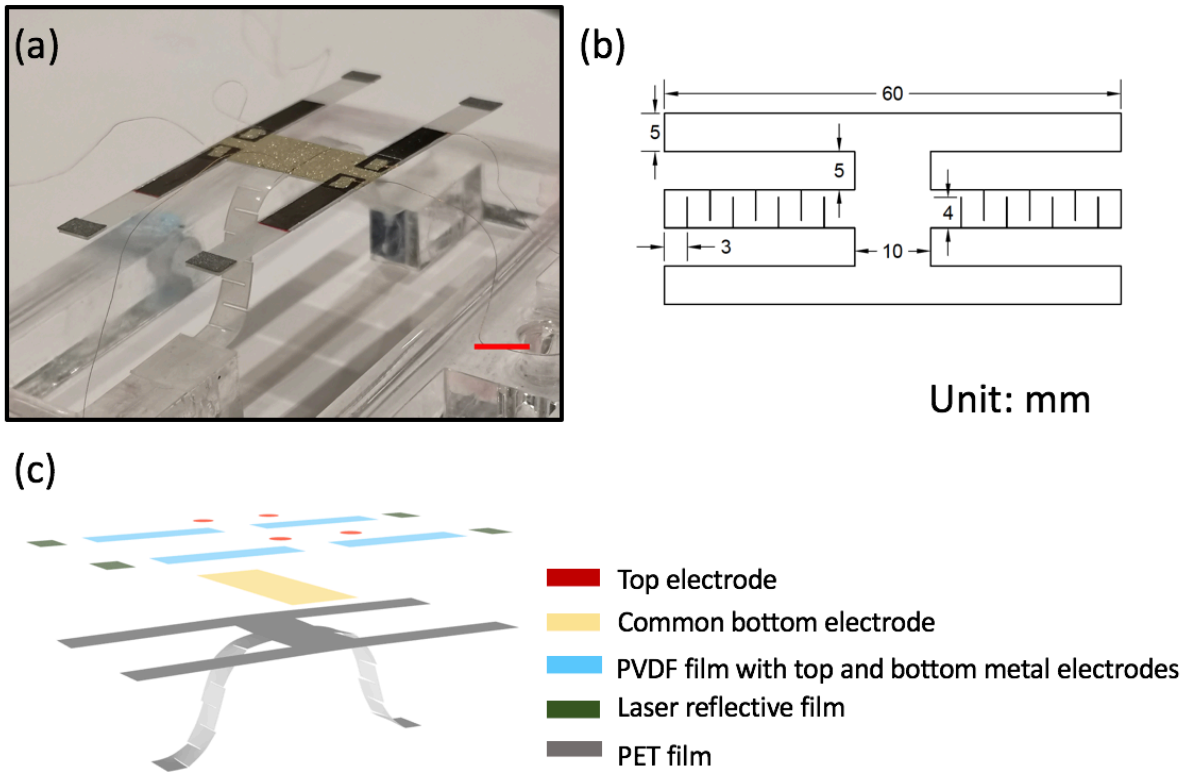
(a)
(b)
60
5
5
4
3
10
Unit: mm
(c)
Top electrode
Common bottom electrode
PVDF film with top and bottom metal electrodes
Laser reflective film
PET film

Fig. 5

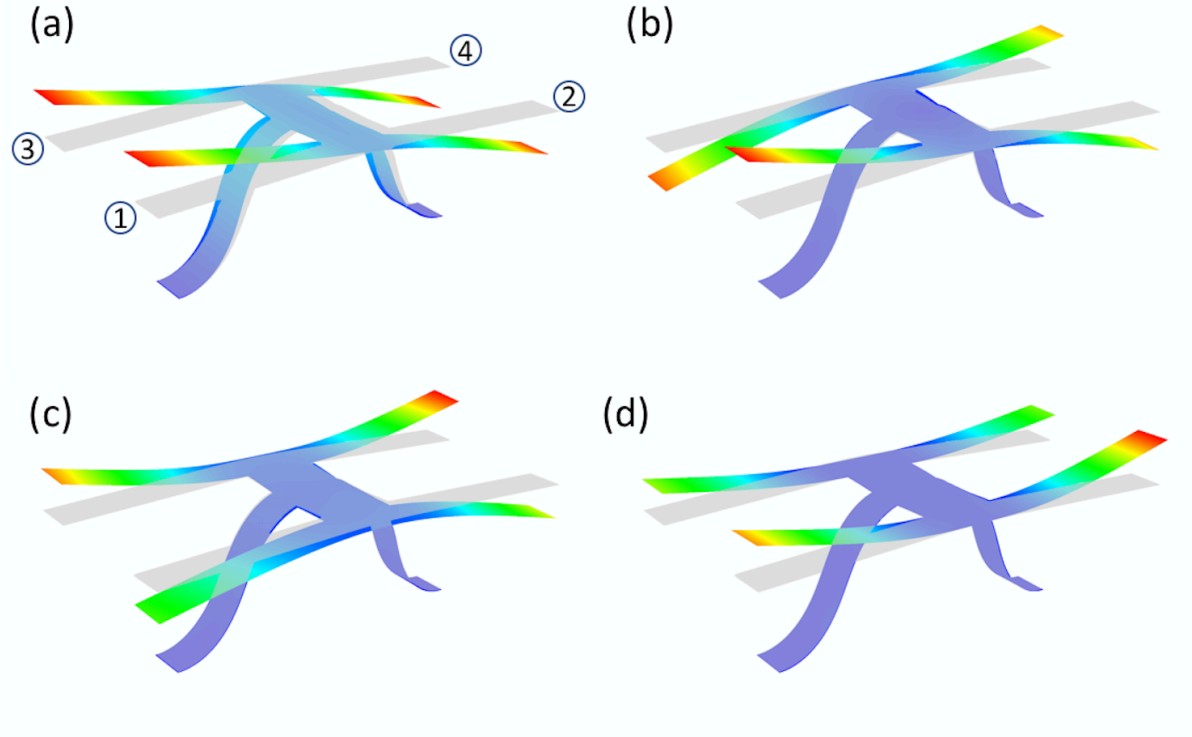

Fig. 6

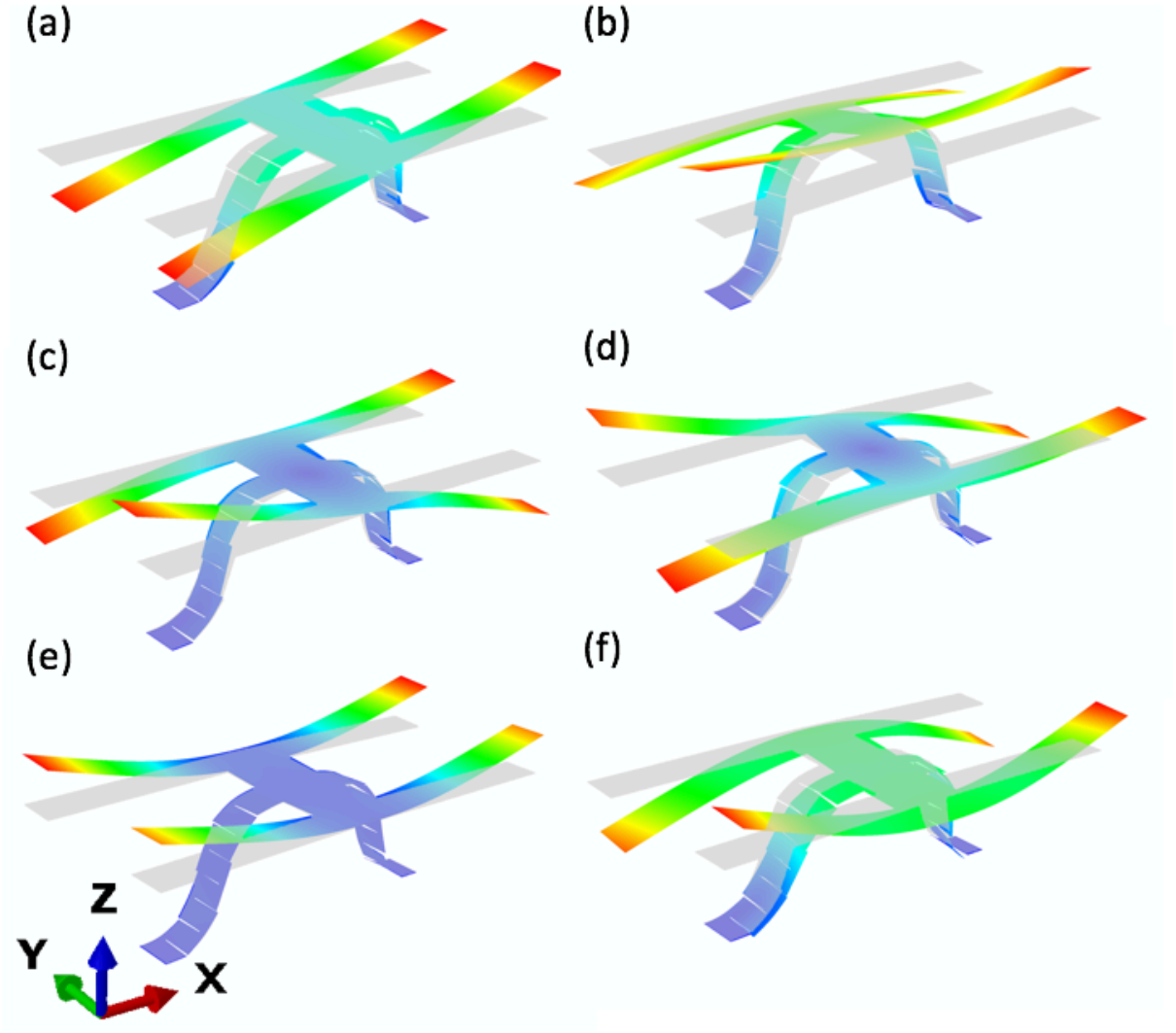

Fig. 7

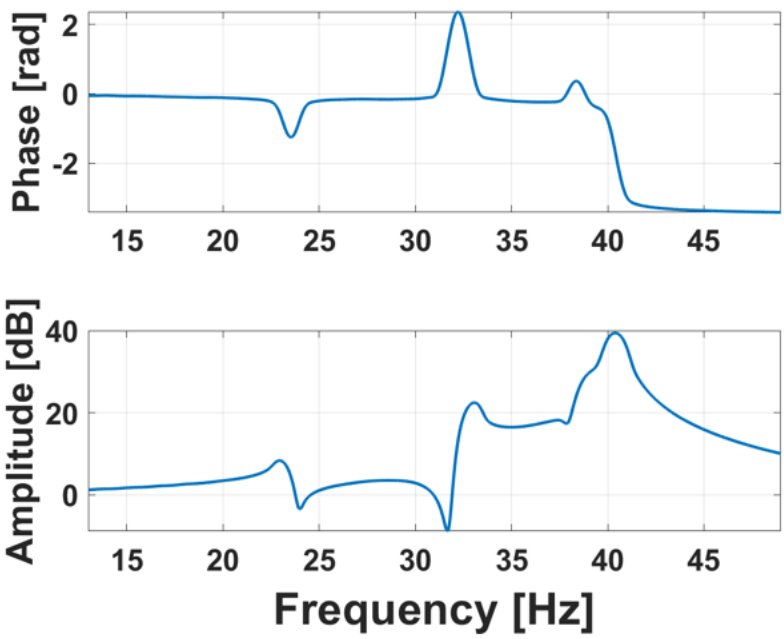
Phase [rad]
2
0
-2
15
20
25
30
35
40
45
Amplitude [dB]
40
20
0
15
20
25
30
35
40
45
Frequency [Hz]

Fig. 8

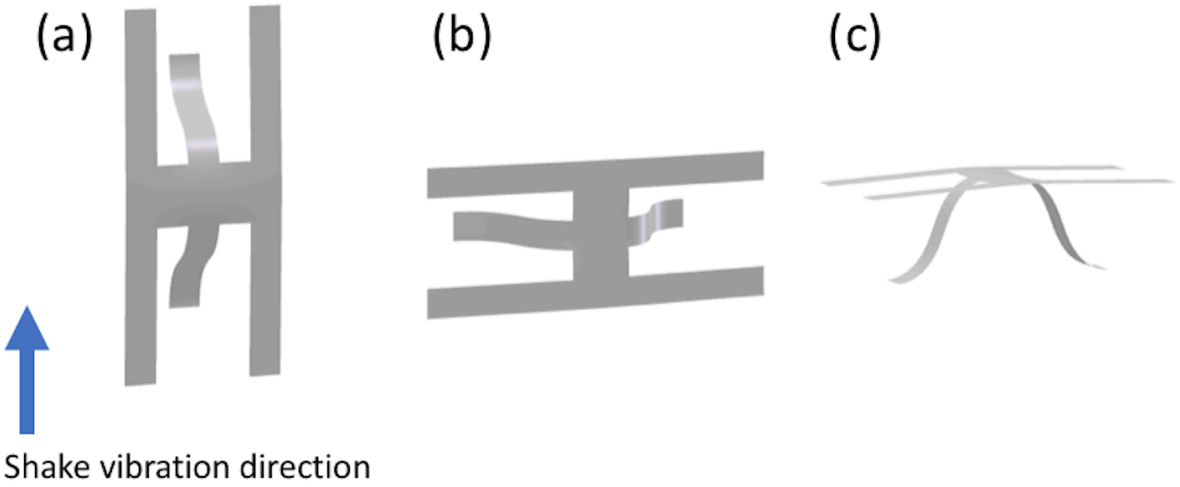
(a)
(b)
(c)
Shake vibration direction

Fig. 9

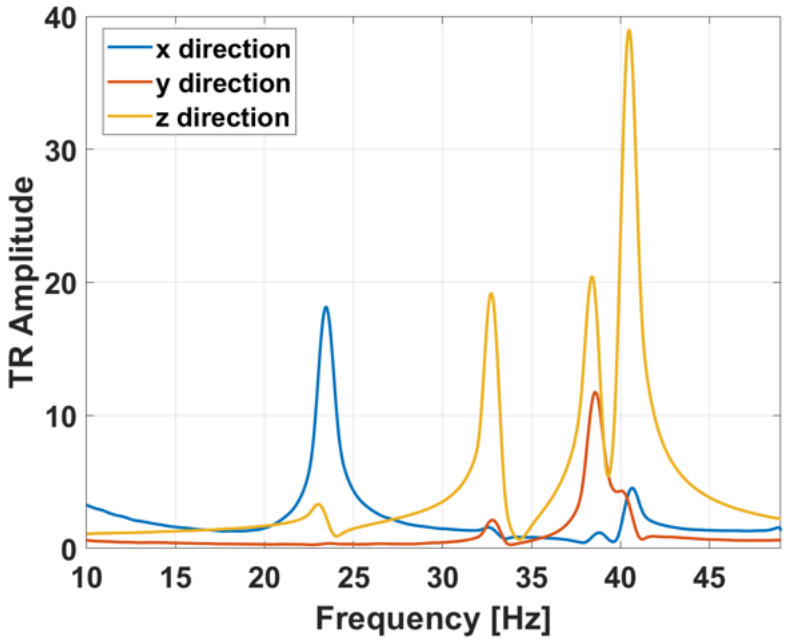
x direction
y direction
z direction
TR Amplitude
Frequency [Hz]

Fig. 10

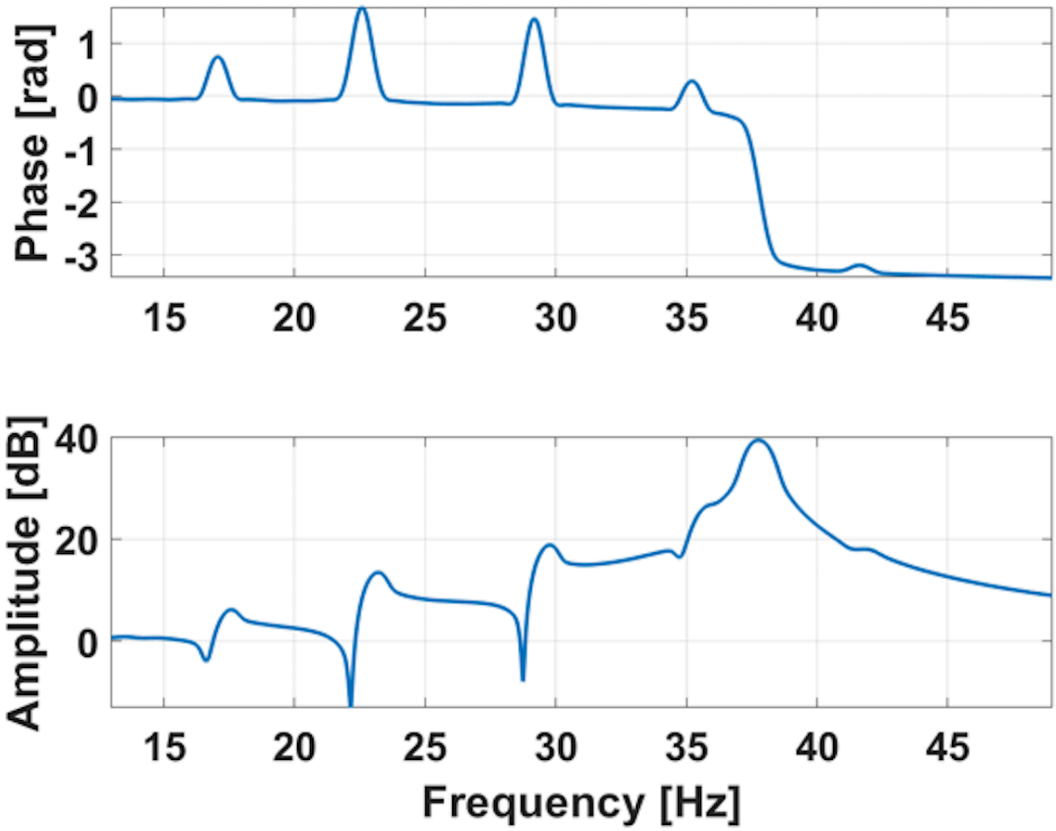
Phase [rad]
Amplitude [dB]
Frequency [Hz]

Fig. 11

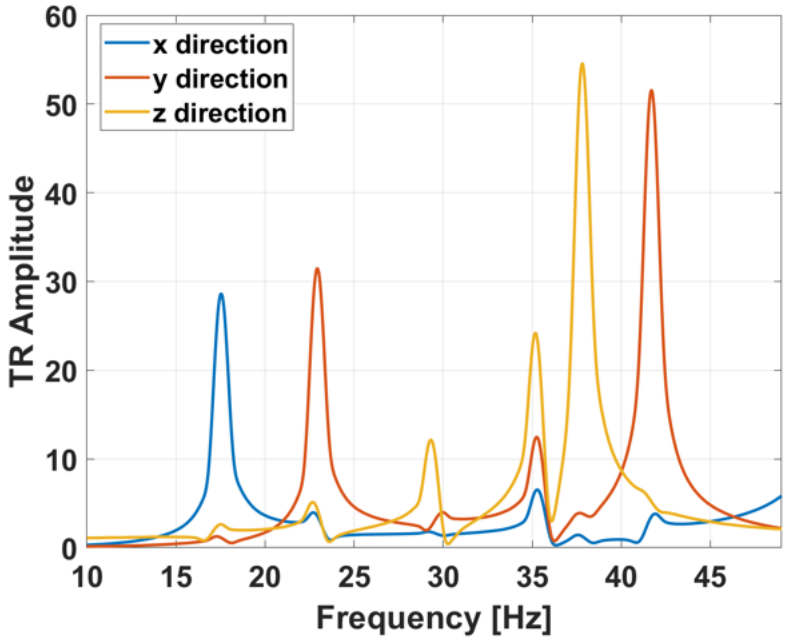
x direction
y direction
z direction
TR Amplitude
Frequency [Hz]
0
10
20
30
40
50
60
10
15
20
25
30
35
40
45

Fig. 12

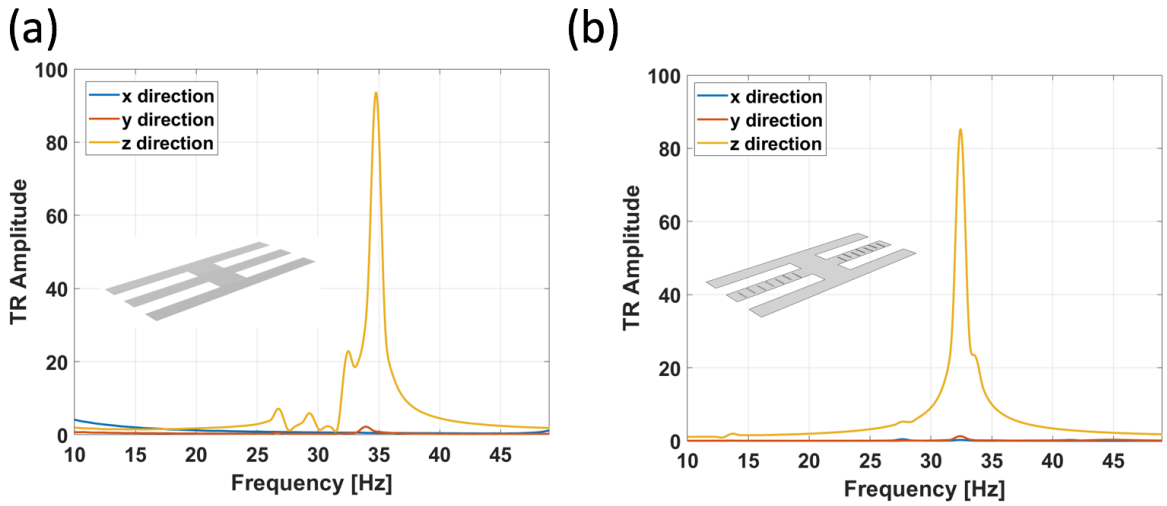
(a)
(b)
x direction
y direction
z direction
TR Amplitude
Frequency [Hz]
0
20
40
60
80
100
10
15
20
25
30
35
40
45

Fig. 13

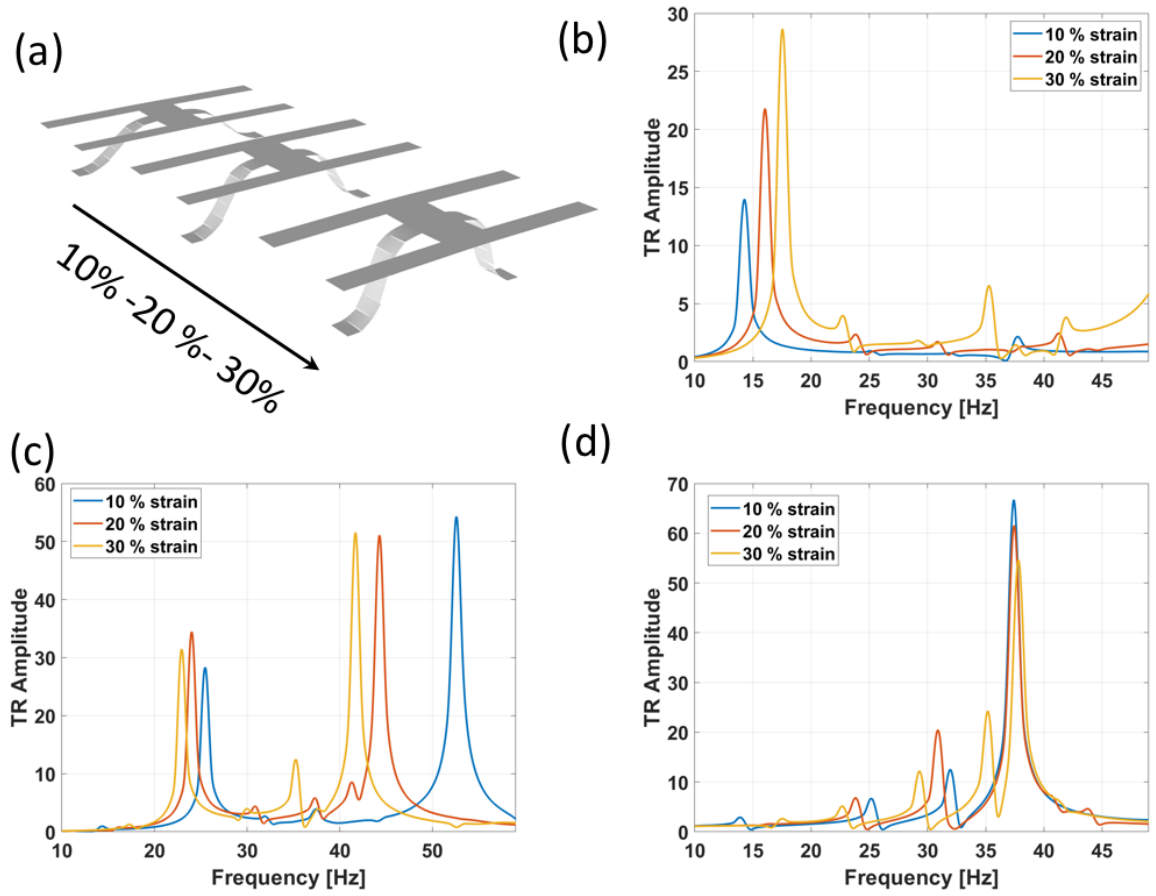
(a)
10% -20 %- 30%
(b)
10 % strain
20 % strain
30 % strain
TR Amplitude
Frequency [Hz]
(c)
10 % strain
20 % strain
30 % strain
TR Amplitude
Frequency [Hz]
(d)
10 % strain
20 % strain
30 % strain
TR Amplitude
Frequency [Hz]

Fig. 14

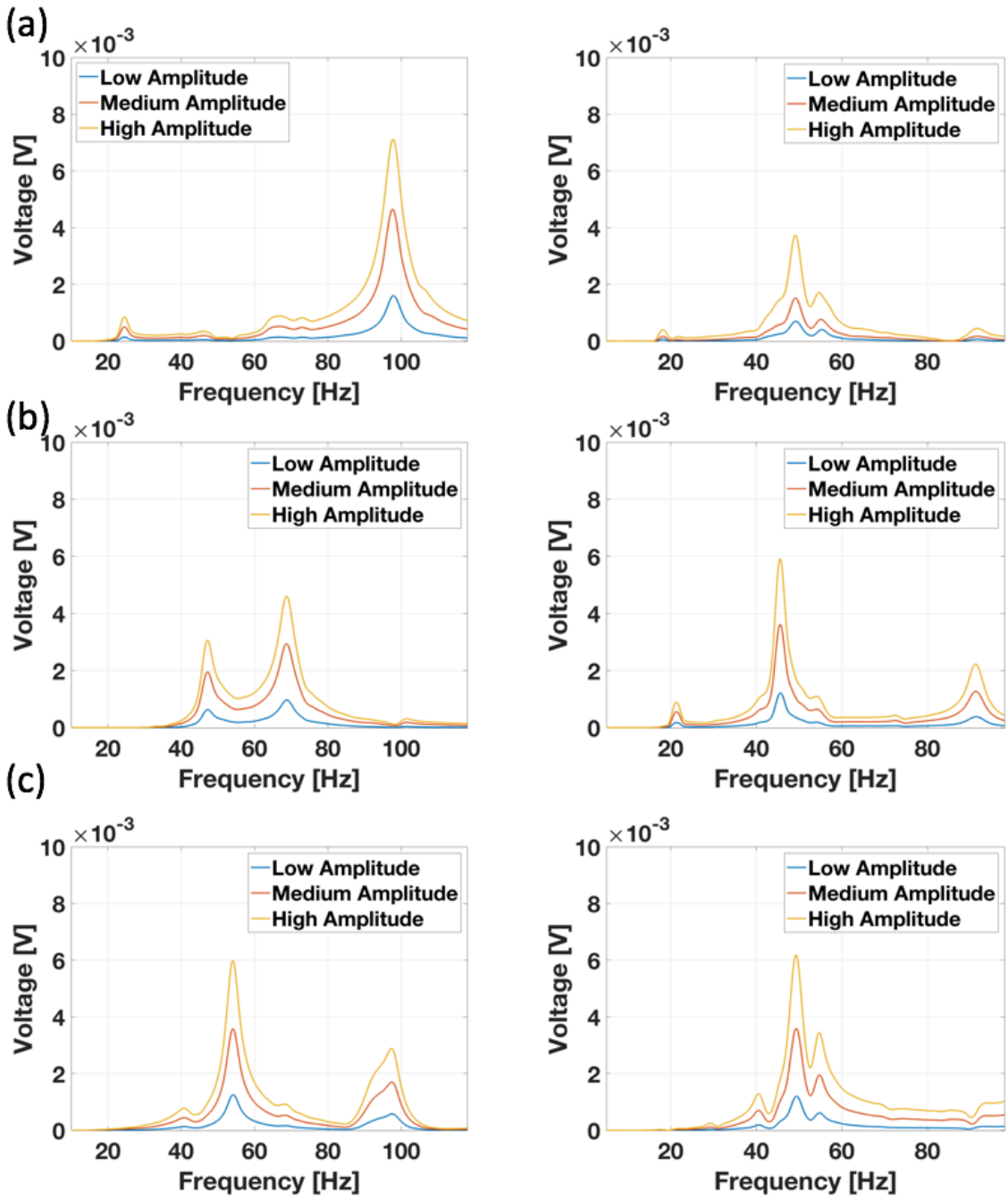
(a)
(b)
(c)
×10^-3
Voltage [V]
Frequency [Hz]
Low Amplitude
Medium Amplitude
High Amplitude

Fig. 15

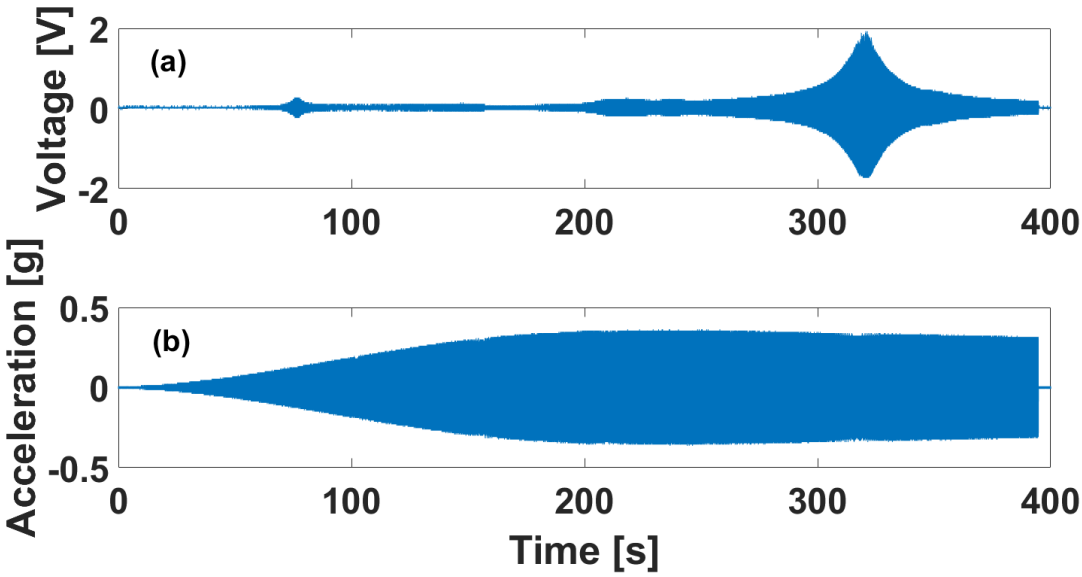
(a)
(b)
Voltage [V]
Acceleration [g]
Time [s]
2
0
-2
0.5
-0.5
0
100
200
300
400

Fig. 16

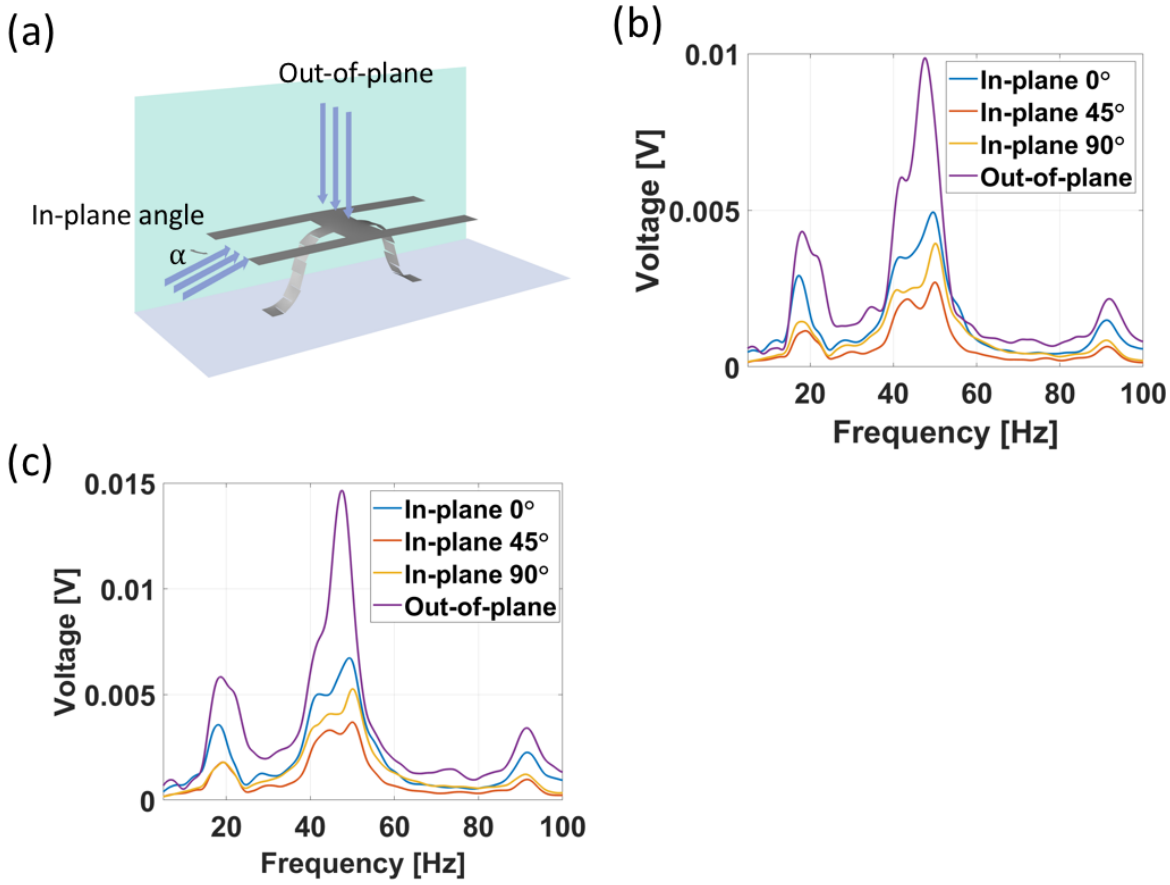
(a)
Out-of-plane
In-plane angle
α
(b)
Voltage [V]
Frequency [Hz]
In-plane 0°
In-plane 45°
In-plane 90°
Out-of-plane
0.01
0.005
0
20
40
60
80
100
(c)
Voltage [V]
Frequency [Hz]
In-plane 0°
In-plane 45°
In-plane 90°
Out-of-plane
0.015
0.01
0.005
0
20
40
60
80
100

Table 1.

Direction	Metastructure w/o cuts		Metastructure w/ cuts	
	Position 1	Position 2	Position 1	Position 2
x	-0.0153	0.453	-0.0133	0.108
y	-0.0311	0.262	-0.0169	0.0781
z	-0.0579	-0.175	-0.0233	-0.0605

Table 2

Mode	FEA	Test
1	24.9 Hz	24 Hz
2	33.9 Hz	32 Hz
3	38.2Hz	38 Hz
4	39.6 Hz	40 Hz

Table 3

Mode	FEA	Test
1	18.9 Hz	17 Hz
2	24.1 Hz	23 Hz
3	30.5 Hz	29 Hz
4	37.5 Hz	35 Hz
5	37.6 Hz	38 Hz
6	43. 3 Hz	42 Hz